Terahertz-assisted excitation of the 1.5mm photoluminescence of Er in crystalline Si

Moskalenko, A.S.; Yassievich, I.N.; Forcales Fernandez, M.; Klik, M.A.J.; Gregorkiewicz, T.

Published in:
Physical Review B

Terahertz-assisted excitation of the 1.5-μm photoluminescence of Er in crystalline Si

A. S. Moskalenko and I. N. Yassievich
A. F. Ioffe Physico-Technical Institute, Politekhnicheskaya 26, St. Petersburg, 194021 Russia

M. Forcales, M. Klik, and T. Gregorkiewicz
Van der Waals-Zeeman Institute, University of Amsterdam, Valckenierstraat 65, NL-1018 XE Amsterdanm, The Netherlands
(Received 25 February 2003; revised manuscript received 8 September 2003; published 5 October 2004)

We show that the 1.5-μm emission from Si:Er generated by continuous-mode band-to-band optical excitation can be dramatically enhanced by terahertz radiation from a free-electron laser. The effect is observed at cryogenic temperatures in samples prepared from FZ-Si by high-temperature implantation with Er ions and requires a high density of infrared photons ($\hbar\Omega \approx 100$ meV). Based on experimental characteristics of this effect, we argue that the excitation mechanism responsible for the enhancement is, in this case, different from the previously discussed free-electron-laser-induced optical ionization of trapped carriers. A theoretical model of the energy transfer path is developed. It involves participation of a higher-lying conduction $c2$ band of the Si host and excitation into the $^4I_{11/2}$ second excited state of Er^{3+} ion. Since formation of the Er-related level is not necessary in this mechanism, it opens a possibility to excite a large fraction of Er^{3+} ions, including also these which are not linked to a recombination level in the band gap. Possible implications of the proposed model toward realization of a true three-level scheme in Si:Er are pointed out. Finally, further experiments necessary for testing and confirmation of the theoretically developed model are proposed.

DOI: 10.1103/PhysRevB.70.155201 PACS number(s): 78.66.Db, 61.72.Tt, 41.60.Cr

I. INTRODUCTION

Importance of Er doping as a method of circumventing the lack of optical activity of crystalline silicon (c-Si) is growing and practical Si:Er-based devices are successfully developed—see, e.g., Ref. 1 for an overview. The currently recognized energy transfer mechanisms responsible for activation Er photo- (PL) and electroluminescence—electron-hole recombination at an Er-related shallow level and a hot carrier impact[2]—excite Er^{3+} ion into the $^4I_{13/2}$ first excited state. In this way a true three-level excitation scheme enabling population inversion and lasing is not realized.

Previous investigations revealed that, at cryogenic temperatures, the 1.5-μm Er-related emission from Si:Er can be induced by a mid-infrared (THz frequency range) pulse from a free-electron laser (FEL) applied shortly after initial band-to-band excitation.[3] The microscopic mechanism of the FEL-induced Er emission has been identified as recombination of a hole optically ionized from a shallow trap populated by the pump pulse with an electron localized at an Er-related level in the bandgap.[4] Subsequently, it has been found that this phenomenon is related to the afterglow of slowly decaying emission[5] appearing as a result of thermalization of shallow traps. In addition, it was shown[6] that a FEL-induced enhancement of the Er-related emission appears also under conditions of continuous (cw) band-to-band pumping, when a steady-state population of carriers at shallow traps is reached. In such a case, the magnitude of the PL enhancement was measured to be proportional to the square root of excitation density, over 4 orders of magnitude of FEL power: $I_{PL} \sim \sqrt{P_{FEL}}$.

In the current contribution, we report observation of an experimental fingerprint of another FEL-induced excitation mechanism of Er^{3+} ions in Si. It has been observed at $T = 4.2$ K under conditions of cw band-to-band pumping and high-power THz illumination, for samples prepared by high-temperature implantation of Er ions into n-type FZ-Si substrates. Such a sample choice follows from consideration of the crystalline quality of the material. Although in FZ material emission from an Er^{3+} ion is known to be weaker than in optimized oxygen-rich samples, the high substrate quality combined with the low implantation damage related to the elevated temperature of implantation is likely to result in a superior crystalline quality of the samples, making them ideal for investigations of energy transfers. In contrast to the earlier discussed one, this new excitation path is characterized by a linear dependence on the FEL radiation density. Triggered by these findings, we propose a theoretical model for this new excitation mechanism which accounts for the experimental data. It is similar to that discussed in Ref. 7 and involves participation of a higher-lying $c2$ conduction band of the silicon host and the $^4I_{11/2}$ second excited state of the Er^{3+} ion. The excitation does not proceed via a level in the Si bandgap. In that way, this mechanism is very different from the excitonic Auger mediated energy transfer which can be realized only for Er-related centers forming such levels—typically for ~1% of the total Er concentration. The process requires high-energy free carriers, and therefore, its efficiency depends on the lifetime of free carriers generated optically by band-to-band illumination. In the proposed excitation scheme, a true three-level system is realized (presently possible only in nanocrystalline Si but not in crystalline bulk Si) where the second $^4I_{11/2}$ excited state of Er^{3+} ion becomes populated. While the present study is clearly of fundamental character, it is interesting to note that eliminating the bandgap level from the energy transfer should disable the *so-called* back-transfer process of excitation reversal. Since the back-transfer is generally held responsible for thermal quenching of Si:Er emission, the proposed excitation mecha-

nism gives new hopes for realization of efficient room-temperature PL based on Si:Er material, a crucially important aspect in view of device applications.

II. EXPERIMENTAL

Intense mid-infrared radiation ($\nu \approx 30$ THz) for the current experiment was provided by a free-electron laser. Therefore, the experiment has been conducted at the Free Electron Laser for Infrared eXperiments (FELIX) users facility of the FOM Institute for Plasma Physics "Rijnhuizen" in the Netherlands. The FELIX delivers infrared macropulses with a repetition rate of 5 Hz and duration of approximately 5 μs. Each macropulse contains a train of micropulses of ≈ 1.7 ps duration and repetition rate of either 25 MHz or 1 GHz. The energy carried by a macropulse is chosen by selecting the repetition rate of micropulses and adjusting their amplitude by attenuators (up to 30 dB) inserted into the infrared beam.

In the correlated two-beam experiment the Si:Er sample (FZ-Si, *n*-type, implanted at 500 °C with 1100 keV Er ions to a total dose of 10^{13} cm^{-2}—Ref. 8 for details on sample preparation and PL spectrum) is placed in a variable temperature cryostat and excited with above bandgap light and, simultaneously, exposed to the THz beam from the FEL. The primary optical excitation is provided by a cw operating solid state laser at a wavelength of $\lambda_{cw} = 820$ nm with ≈ 10 mW power. In the experiment, we followed the influence of the FEL beam tuned to the wavelength around $\lambda_{FEL} \approx 10$ μm, for which the maximal dynamic range is available on the most intense part of the Er-related PL spectrum selected by a 20 nm band-pass filter centered at the strongest spectral component at 1549 nm.

III. EXPERIMENTAL RESULTS

Upon cw illumination by the pump laser an equilibrium situation is created. That means that a steady-state concentrations at all stages of the excitation process are reached. Under conditions of this experiment—low temperature, high density pumping—these will include free carriers in the bands, carriers bound at available traps, free and bound excitons, and Er^{3+} ions in the ground and the excited states. In that way a steady-state Er-related emission at $\lambda \approx 1.5$ μm is achieved. This equilibrium emission is perturbed by additional laser pulse and restores to the equilibrium value when the pulse is terminated. Experiments performed with low power FEL pulses showed quenching of PL intensity. Such a behavior is consistent with our earlier findings for a pulsed band-to-band excitation regime (pumping with the second harmonics of the Nd:YAG laser) where quenching of PL intensity was observed when the FEL pulse of 25 MHz repetition rate was applied coincident with the Nd:YAG.[9] The present experiments were performed with the 1 GHz FEL repetition rate, corresponding to the 40 times higher energy of the FEL macropulse (up to ~ 60 mJ).

Figure 1 summarizes the most important experimental results of the current study. The zero level of the vertical scale corresponds to the steady-state Er-related PL, as obtained under cw illumination. The first peak represents response of

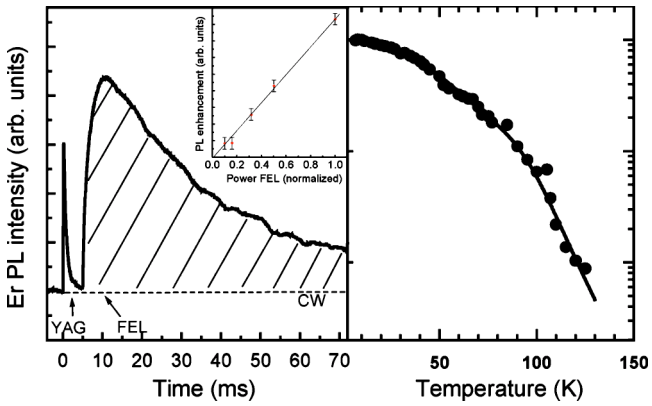

FIG. 1. Dynamics of the Er PL at a temperature $T \approx 5$ K under illumination with a Nd:YAG and a FEL with a delay of 5 ms respect the Nd:YAG. The dashed line is the steady-state level of the 1.5-μm emission generated by cw illumination from a diode (820 nm). The inset shows the dependence of the THz-assisted excitation (PL enhancement) of Er^{3+} ions as a function of the FEL power (normalized). The solid line is a guide for the eye. In the second panel, temperature dependence of PL intensity observed in the investigated material is given.

the sample to a short (ns) pulse from the Nd:YAG laser ($\lambda_{YAG} = 532$ nm). As can be seen, Er-related emission increases following the additional band-to-band excitation and then decays towards the equilibrium value with a time constant of $\tau \approx 0.80$ ms characteristic for the lifetime of the excited state of Er^{3+} ion, as expected. The sample response to a high energy FEL pulse, represented by the second peak, is quite different; its magnitude is bigger (comparable to the equilibrium PL level generated by pumping in the visible), and its kinetics is much slower than that of the PL signal induced by Nd:YAG. In order to check whether the enhancement is not due to a small increase of sample temperature, which might be induced by the powerful FEL pulse, we investigated thermal quenching of PL intensity in the sample used in the present study. The result, depicted in the right panel of Fig. 1, shows that only a monotonous lowering of the amplitude of PL signal is seen at higher temperatures.

In the inset to the figure, the integrated value of the additional PL signal appearing upon FEL pulse is plotted as a function of THz excitation density (normalized). As can be concluded, the enhancement effect varies linearly with power and does not show saturation within the studied FEL power range. The different dependence on the macropulse power ($I_{PL} \sim P_{FEL}$) indicates that this enhancement effect is due to a different physical mechanism than the trap-ionization-related enhancement identified and discussed in Ref. 4 for the more "standard" Cz-Si:Er material. We propose that the additional PL appearing for large FEL powers represents a manifestation of a thus far unknown excitation path which can be induced by high-power THz radiation and active exclusively at cryogenic temperatures in high-quality FZ material. (We note that oxygen-lean material is not usually used for preparation of Si:Er photonic structures, as high oxygen content is known to improve efficiency and thermal stability of Er emission in crystalline Si matrix).

We have also looked how the observed enhancement effect was changing upon temperature increase. We have ob-

served that magnitude of the additional luminescence was gradually decreasing, and no enhancement could be observed at $T>40$ K. At the same time, PL quenching[4] visible also at low temperatures for small FEL fluxes was becoming dominant. Therefore, it cannot be decided at the moment whether the observed thermal reduction of PL intensity represents an inherent feature of the MIR-induced excitation, or results from competition with the quenching. It is not clear whether this question can be resolved experimentally, as the two effects are entangled.

IV. THEORETICAL CONCEPT OF A NEW EXCITATION MECHANISM

Upon cw diode excitation we have stationary concentration of free electrons (n) and holes (p), which results in stationary concentration of excited Er^{3+} ions and the time-independent PL intensity. We propose that application of THz radiation opens an additional excitation channel for Er^{3+} ions embedded in c-Si. The energy quantum $\hbar\Omega$ of THz radiation is absorbed by an electron and then the recombination of the electron-hole pair assisted by Auger excitation of Er^{3+} from state $^4I_{15/2}$ to state $^4I_{11/2}$ takes place. The excitation is possible only if $\hbar\Omega+E_g$ (E_g is the band gap energy of silicon) is larger than the energy difference $\Delta_{ff'}\approx 1.24$ eV between these states. Such a process can be described by the second order perturbation theory and involves transition through a virtual electron state.

The proposed mechanism is based on a model of c-Si band structure adopted in Refs. 10 and 11—see Appendix A for details. We use a simplified approach, where the spin-orbit interaction is neglected and the heavy and the light hole bands coincide, therewith forming a heavy hole band h, and the split-off band plays a role of a light hole band l. Therefore, the heavy hole band h is doubly degenerated in $\vec{k}$ and the light hole band l is nondegenerated in $\vec{k}$. The double degeneration in spin should be also taken into account. The wave functions of band h are polarized perpendicular to $\vec{k}$, whereas the wave functions of band l are polarized parallel to $\vec{k}$. For conduction bands it is enough to consider only the first two subbands $c1$ and $c2$. The resulting band structure is shown in Fig. 2. The introduced simplifications should not considerably affect the results of the following calculations.

The energy quantum of the terahertz radiation is not large enough for a direct transition of an electron from the bottom of the first $c1$ to the second $c2$ conduction band. However, if the excited electron immediately recombines with a hole in an Auger process with participation of an Er^{3+} ion, the exact energy conservation at the intermediate stage is not required. The momentum and the energy released by the electron-hole recombination are then transferred to an Er^{3+} ion. Such a transfer is effective if the released energy is sufficient for excitation of an Er^{3+} ion, in this case into the second excited state. It is known that transitions between the ground and the second excited states of Er^{3+} ions in insulating hosts involve phonons,[12] in contrast to excitations into the first exited state. Therefore, we may involve phonons to compensate for the energy difference appearing in the excitation process.

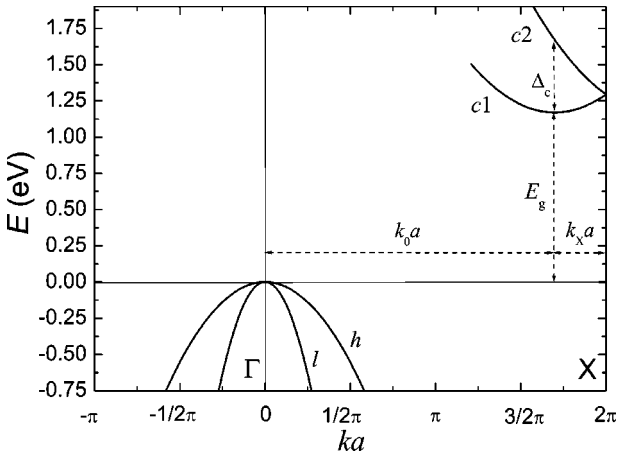

FIG. 2. Scheme of the energy bands of Si. Two lowest conduction bands $c1$ and $c2$, and two upper valence bands h,l are shown. The band gap is $E_g=1.17$ eV, $\Delta_c=0.5$ eV, $a=5.43$ Å is the lattice constant of Si, $k_0=0.85(2\pi/a)$, $k_X=0.15(2\pi/a)$.

Phonons will also enable a fast relaxation from the second to the first excited state.

In fact, there could be two possible realizations of such an Auger process induced by THz radiation:

1. An electron from conduction band $c1$ [see Fig. 3(a)] gains energy by absorbing a THz photon $\hbar\Omega$ and goes to conduction band $c2$, from where it recombines with a heavy hole and excites the Er^{3+} ion into the $^4I_{11/2}$ state via Coulomb interaction. At this stage phonons take part in the process. The electron state in the $c2$ subband is virtual.

2. A heavy hole in band h absorbs a photon and goes into a virtual state in band l. Then it recombines with an electron from band $c1$ transferring energy to an Er^{3+} ion and to phonons [see Fig. 3(b)].

Because of zero overlap integral between the top of valence band and the bottom of $c1$, the second recombination process occurs due to admixture of $c2$ states into $c1$, which appears only for nonzero electron energies. This leads to an additional vanishing factor in the expression for the probability of such a process. Therefore, the second excitation path can be neglected in comparison to the first one.

The probability of excitation of an Er^{3+} ion can be written as

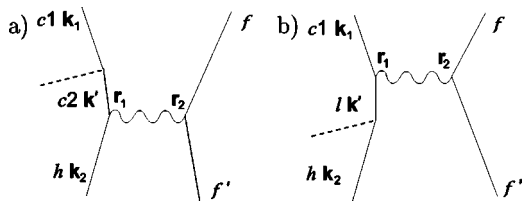

FIG. 3. Feynman diagrams for two possible processes which lead to transition of erbium ions to the second excited state ($^4I_{11/2}$). Both transitions are stimulated by means of terahertz radiation. See text for details.

$$W_{\mathrm{ex}} = \frac{2\pi}{\hbar} N_\Omega \sum_{1,2} |t_{21}|^2 f_e(\varepsilon_1) f_h(\varepsilon_2) \sum_{N,N_\mathrm{i}} |\langle L_\mathrm{f}, N_\mathrm{i} + N | L_\mathrm{i}, N_\mathrm{i}\rangle|^2 P(N_\mathrm{i}) \times \delta(E_g + \varepsilon_1 + \varepsilon_2 + \hbar\Omega - \Delta_{ff'} - N\hbar\omega). \quad (1)$$

Here the initial electron state $|1\rangle = |\vec{k} s_1\rangle$ is an electron in the ν^{th} valley of the conduction band $c1$ with momentum $\hbar(\vec{k}_{\nu 0} + \vec{k}_1)$ (wave vector $\vec{k}_{\nu 0}$ corresponds to the bottom of the ν-valley of the conduction band) and spin $s_1 (s_1 = \pm 1/2)$. The final state $|2\rangle = |\vec{k}_2 p_2 s_2\rangle$ is an electron state in the valence band with momentum $\hbar\vec{k}_2$, polarization p_2 (there are two possible polarizations in the heavy hole subband), and spin $s_2 (s_2 = \pm 1/2)$. t_{12} is the matrix element of electron transition between states $|1\rangle$ and $|2\rangle$. $\varepsilon_1, \varepsilon_2$ are electron and hole kinetic energies in states $|1\rangle$ and $|2\rangle$, correspondingly, and $f_e(\varepsilon_1), f_h(\varepsilon_2)$ are distribution functions of electrons and holes in these states. The sum $\Sigma_{1,2}$ is taken over all possible electron and hole states. The second sum Σ_{N,N_i} is taken over states of vibrational system of the Er^{3+} ion. N_i is the number of phonons in initial state, $N = N_\mathrm{f} - N_\mathrm{i}$ is the difference in phonon number between final L_f and initial L_i state of the ion vibrational system, and $P(N_\mathrm{i})$ is the probability of having N_i phonons in the initial state. N_Ω is the number of photons, Ω is the frequency of terahertz radiation.

The phonon part in Eq. (1)

$$J(N) = \sum_{N_\mathrm{i}} |\langle L_\mathrm{f}, N_\mathrm{i} + N | L_\mathrm{i}, N_\mathrm{i}\rangle|^2 P(N_\mathrm{i}), \quad (2)$$

was calculated in the model of two shifted identical parabolic adiabatic potentials.[13] For low temperature $kT \ll \hbar\omega$, where ω is the frequency of local vibrations, we have

$$J(N) = S^N \exp(-S) \frac{1}{N!}. \quad (3)$$

Here S is the Huang-Rhys factor

$$S = \frac{\Delta^{\mathrm{opt}}_{f'f} - h\nu_{f'f}}{2\hbar\omega}, \quad (4)$$

where $\Delta^{\mathrm{opt}}_{f'f}$ is the energy of optical absorption for transition $f \to f' ({}^4\mathrm{I}_{15/2} \to {}^4\mathrm{I}_{11/2})$ and $h\nu_{f'f}$ is the energy of luminescence.

The square of the electron transition matrix element $|t_{21}|^2$ can be written as

$$|t_{21}|^2 = \left| \sum_{\vec{k}'s'} \frac{\langle \vec{k}_2 p_2 s_2; f' | \hat{V}_c | \vec{k}' s'; f\rangle \langle \vec{k}' s' | \hat{H}_{e-r} | \vec{k}_1 s_1\rangle}{\varepsilon_1(\vec{k}_1) + \hbar\Omega - \varepsilon'(\vec{k}')} \right|^2. \quad (5)$$

The optical transition matrix element $\langle \vec{k}' s' | \hat{H}_{e-r} | \vec{k}_1 s_1\rangle$ is calculated in Appendix C

$$|\langle c1, \nu, \vec{k}' s' | \hat{H}_{e-r} | c2, \nu, \vec{k}_1 s_1\rangle|^2 = \frac{2\pi}{\kappa_\infty \hbar\Omega V} \frac{e^2\hbar^4}{m'^2} \frac{1}{3} k^2_{1\perp\nu} \delta_{\vec{k}_1, \vec{k}'} \delta_{s1,s'}. \quad (6)$$

Here κ_∞ is dielectric constant of Si in the high frequency limit, V is normalization volume, $\vec{e}$ is vector of light polarization, m' is an unknown mass, for which there is a limitation $m' \gtrsim 0.1\, m_\perp$ (see Appendix A). $\vec{k}_1, \vec{k}'$ are counted from the bottom of the valley ν of conduction band $c1$, and $k_{1\perp\nu}$ is the length of the transverse component of $\vec{k}_1$.

Calculation of the matrix element corresponding to Coulomb interaction is performed following Ref. 14:

$$|\langle h, \vec{k}_2 p_2 s_2; f' | \hat{V}_c | c2, \nu, \vec{k}_1 s_1; f\rangle| = \frac{1}{V} \left(\frac{4\pi e^2}{\kappa(\Delta_{f'f}/\hbar, k_0) k_0^2} \right) |\langle u^h_{\vec{k}_2 p_2 s_2} | u^{c2,\nu}_{\vec{k}_{0\nu} s_1}\rangle| |\langle f' | e^{i\vec{k}_{0\nu}\vec{r}} | f\rangle|, \quad (7)$$

where $u^h_{\vec{k}_2 p_2 s_2}$ and $u^{c2,\nu}_{\vec{k}_{0\nu} s_1}$ are the Bloch amplitudes of corresponding electron states. It has also been considered that in the process of Auger excitation in Si a large momentum, of order $\hbar k_0$, is transferred to the f-electron. In Eq. (7) the time and spatial dispersion of the dielectric constant $\kappa(\omega, k)$ is also taken into account. Expression (7) is really independent of ν and momentum of hole $\vec{k}_2$.

Because of a relatively small value $k_0 r_f = 0.4$, where r_f is the radius of the f-shell of an erbium ion, we expand the factor $e^{i\vec{k}_{0\nu}\vec{r}}$ in Eq. (7) in series and estimate the first three terms

$$\langle f' | e^{i\vec{k}_{0\nu}\vec{r}} | f\rangle = \langle f' | f\rangle + i\vec{k}_{0\nu} \langle f' | \vec{r} | f\rangle - \sum_{ij} \frac{k_{0\nu i} k_{0\nu j}}{2} \langle f' | r_i r_j | f\rangle + \cdots. \quad (8)$$

The first term at the right hand side of Eq. (8) is equal to zero and in the second term we have dipole matrix element for optical transition

$$\vec{d}_{f'f} = \langle f' | \vec{r} | f\rangle, \quad (9)$$

which average value $\overline{d_{f'f}}$ can be estimated through the corresponding oscillator strength P for unpolarized light[15]

$$P = \chi \frac{1}{3(2J+1)} \sum_{ff'} \frac{2m_0 \Delta_{f'f}}{\hbar^2} d^2_{f'f}, \quad (10)$$

where $(2J+1) = 16$ is the number of states in multiplet ${}^4\mathrm{I}_{15/2}$, χ is the refractive index of the medium, in which erbium ions are embedded. We use values of the oscillator strength for the ${}^4\mathrm{I}_{15/2} \to {}^4\mathrm{I}_{11/2}$ transition for different crystals $P = 0.2 - 0.6 \cdot 10^{-6}$,[15,16] $\chi \approx 3.5$, and we can estimate

$$\overline{d_{f'f}} \simeq r_f \beta, \quad (11)$$

where the numerical factor β is of the order of 10^{-3}.

On the other side, using the symmetry properties of f-states we get for the third term in Eq. (8)

$$\sum_{i,j} \frac{k_{0\nu i} k_{0\nu j}}{2} \langle f' | r_i r_j | f\rangle = \frac{k_0^2}{2} \langle f' | z^2 | f\rangle. \quad (12)$$

We see that in the considered situation the third term is dominant because $\langle f' | z^2 | f\rangle \simeq r_f^2$ and $k_0 r_f \gg \beta$. In contrast to usual radiative transitions, for the process considered just this term determines the transition probability and not the dipole term. In result we have the following estimation for

the last factor on the right hand side of Eq. (7):

$$\langle f'|e^{i\vec{k}_{0\nu}\vec{r}}|f\rangle \simeq -\frac{k_0^2}{2}\langle f'|z^2|f\rangle. \tag{13}$$

Then $|t_{12}|^2$ can be calculated from Eq. (5) neglecting the difference in electronic kinetic energies in comparison to $\Delta_c-\hbar\Omega$, and taking into account Eqs. (6) and (7). Substituting the result in Eq. (1) we get

$$\begin{aligned} W_{ex} = {} & \frac{2\pi}{\hbar}\rho_\Omega \sum_{\nu s_1}\sum_{p_2 s_2}\frac{V^2}{(2\pi)^6}\int d^3k_1 \int d^3k_2\, f_e(\varepsilon(\vec{k}_1))f_h(\varepsilon(\vec{k}_2)) \\ & \times \sum_N J(N)\,\delta(E_g+\varepsilon(\vec{k}_1)+\varepsilon(\vec{k}_2)+\hbar\Omega-\Delta_{f'f}-N\hbar\omega) \\ & \times \frac{2\pi e^2\hbar^4}{\kappa_\infty \hbar\Omega m'^2}\frac{1}{3}k_{1\perp\nu}^2\frac{1}{(\Delta_c-\hbar\Omega)^2}\frac{1}{V^2}\left(\frac{4\pi e^2}{\kappa k_0^2}\right)^2 \\ & \times |\langle u^h_{\vec{k}_2 p_2 s_2}|u^{c2,\nu}_{\vec{k}_{0\nu} s_1}\rangle|^2 \sum_{f'}\frac{\overline{k_0^4|\langle f'|z^2|f\rangle|^2}}{4}, \end{aligned} \tag{14}$$

where $\rho_\Omega = N_\Omega/V$ is the density of THz photons. In Eq. (14) we have put $\kappa \equiv \kappa(\Delta_{ff'}/\hbar, k_0)\approx 1$, because the screening effect is small for a small distance, of the order of $(k_0)^{-1} \approx 1$ Å, and high frequency (large energy transferred in the Auger process)—for details see Refs. 14 and 17. We should take sum over the final state f' of f-electrons and average over the initial state f. The estimation shows that

$$\sum_{f'}\overline{|\langle f'|z^2|f\rangle|^2} = r_f^4\gamma_f, \tag{15}$$

where the unknown factor γ_f is of the order of 10.

The averaged value of the overlap integral between bands h and $c2$ is calculated in Appendix B and we get

$$\overline{\sum_{p_2 s_2 s_1}|\langle u^h_{\vec{k}_2 p_2 s_2}|u^{c2,\nu}_{\vec{k}_{0\nu} s_1}\rangle|^2} = \frac{4}{3}|\langle Z|xy\rangle|^2, \tag{16}$$

where Z is one of the basis wave functions of representation $\Gamma_{25'}$ having the same symmetry properties as the wave function xy of representation $\Delta_{2'}$. The matrix element $|\langle Z|xy\rangle|$ is equal to 0.75 according to Ref. 10.

Assuming ξ_e and ξ_h to be the Fermi energies of electrons and holes in bands $c1$ and h, respectively, we get in the low temperature limit

$$W_{ex} = 2\pi^4\frac{P}{\tilde{c}A}\frac{e^6}{\kappa^2\kappa_\infty}\frac{1}{(\Delta_{f'f}-E_g)^4}\frac{\hbar\, np\, m_\perp}{m'^2}r_f^4\gamma_f|\langle Z|xy\rangle|^2 F(\hbar\Omega). \tag{17}$$

Here $F(\hbar\Omega)$ is given by the following expression:

$$F(\hbar\Omega) = \frac{(\Delta_{f'f}-E_g)^4}{(\hbar\Omega)^2(\Delta_c-\hbar\Omega)^2}\sum_N J(N) f_N(\delta_N), \tag{18}$$

where

$$f_N(\delta_N) = \int_0^1 dy\sqrt{y}\int_0^1 dx_\perp x_\perp \int_0^{1-x_\perp}\frac{dx_\parallel}{\sqrt{x_\parallel}} \times \delta\left(x_\perp + x_\parallel + \frac{\xi_h}{\xi_e}y - \frac{\delta_N}{\xi_e}\right), \tag{19}$$

with

$$\delta_N = \Delta_{f'f} + N\hbar\omega - E_g - \hbar\Omega. \tag{20}$$

P is the power of FEL, A is the irradiated area and $\tilde{c}$ is the light velocity in Si.

Fermi energies of electrons ξ_e and holes ξ_h are found from concentrations of electrons n and holes p, correspondingly

$$n = \frac{4\sqrt{2}}{\pi^2}\frac{m_\perp\sqrt{m_\parallel}}{\hbar^3}\xi_e^{3/2}, \tag{21}$$

$$p = \frac{4\sqrt{2}}{3\pi^2}\frac{m_h^{3/2}}{\hbar^3}\xi_h^{3/2}. \tag{22}$$

The frequency dependence of numerical factor $F(\hbar\Omega)$ has the form of peaks separated from each other by the phonon energy $\hbar\omega$. The amplitudes of the peaks decrease for higher frequencies. In an experiment, one can expect that these peaks will be broadened due to uncertainty in the phonon energy in the one-mode model, splitting of the multiplets and other reasons.

In order to facilitate an easy comparison with the experiment, the final result for excitation probability can be expressed in a more convenient way as

$$\begin{aligned} W_{\rm ex} = {} & 5\times 10^7 \frac{P}{10\ \text{MW}}\frac{1\ \text{cm}^2}{A}\frac{n}{10^{17}\ \text{cm}^{-3}}\frac{p}{10^{17}\ \text{cm}^{-3}} \\ & \times\left(\frac{m'}{0.1\ m_\perp}\right)^{-2}\frac{\gamma_f}{10}F_s\left[\frac{1}{\text{s}}\right], \end{aligned} \tag{23}$$

where P is the THz radiation power in MW. In order to evaluate the frequency dependent numerical factor F_s, values of the Huang-Rhys factor S and the characteristic energy $\hbar\omega$ of phonons involved in the process are necessary. Unfortunately, these are not known for the specific case considered here—the $^4I_{11/2}$ state of Er^{3+} ion embedded in c-Si matrix. In Fig. 4 we show the wavelength dependence of the F_s numerical factor calculated for the electron/hole concentration of $n=p=10^{17}$ cm^{-3} and Huang-Rhys and phonon values of Er in fluorozirconate glass: $S=0.13$ and $\hbar\omega=57$ meV.[12] In order to demonstrate the dependence of F_s on these parameters, we also show the results of evaluation performed for $S=0.5$ and $\hbar\omega=20$ meV. It should be remarked that the shape of F_s factor is practically independent of free-carrier concentration while its magnitude depends on the concentrations, for equal electron and hole concentrations approximately like $n^{2/3}$.

V. DISCUSSION

Figure 1 provides a direct experimental comparison of the band-to-band (pumping by the second harmonics of a Nd:YAG laser) and THz-radiation-assisted excitation

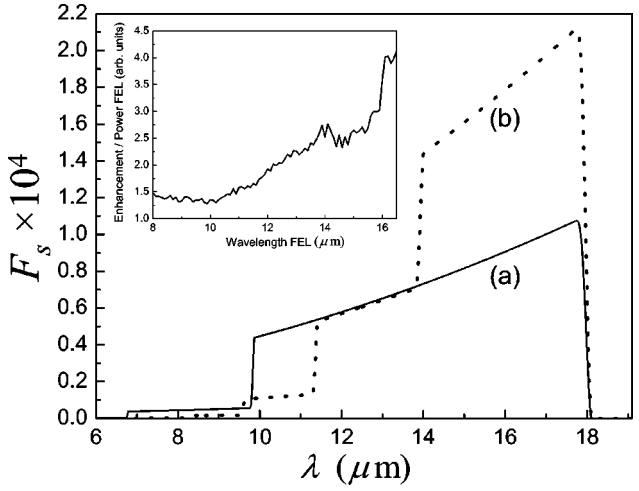

FIG. 4. Dependence of the numerical factor F_s on radiation wavelength λ calculated for $n=p=10^{17}$ cm^{-3} and two different sets of parameters: (a) $S=0.13$ and $\hbar\omega=57$ meV, or (b) $S=0.5$ and $\hbar\omega=20$ meV. For detailed explanation see text. In the inset, preliminary experimental results (the on-going project) on the wavelength dependence of the enhancement effect are given.

mechanisms of the 1.54-μm Er-related emission from the same Si:Er material. In both cases stationary cw illumination takes place. One can see that the THz-induced PL enhancement is more effective. Moreover, the amplitude of the FEL-induced emission is comparable to the level of the steady-state PL generated by the cw band-to-band excitation with the diode laser.

Let us compare the number of erbium ions which can be excited in both cases. For optical band-to-band pumping (Nd:YAG excitation), the effective excitation cross section has been determined as $\sigma\approx10^{-15}$ cm^2.[18] Taking into account the Nd:YAG pulse energy, $P_{\mathrm{YAG}}\sim20$ μJ/pulse and duration $\sim$100 ps we get the photon flux of $\phi=6\times10^{23}$ cm^{-2} s^{-1} (taking typical area of 1 cm^2). Thus the number Er^{3+} ions which will be excited by the Nd:YAG pulse is $\Delta N_{\mathrm{YAG}}\approx0.06N_1$, where N_1 is the number of erbium ions eligible for the band-to-band excitation (i.e., forming a donor level in the gap, thus enabling the energy transfer[19]). According to multiple reports,[20] N_1 corresponds to less than 1% of the total number N_{Er} of Er ions introduced into the sample. In our FZ-Si sample with low oxygen concentration PL intensity is lower than in the Cz-Si:Er. Since we use here the excitation cross section σ as determined for Cz-Si (the value of σ for FZ-Si:Er is not known), we will account for the lower PL intensity by taking the N_1/N_{Er} ratio to be smaller: $N_1/N_{\mathrm{Er}}\approx10^{-3}$. In that way, we estimate the number of Er^{3+} ions which are excited by the Nd:YAG pulse as $\Delta N_{\mathrm{YAG}}\lesssim6\times10^{-5}N_{\mathrm{Er}}$.

Now we will estimate the number of Er^{3+} ions which can be excited by the FEL pulse (ΔN_{FEL}) according to the earlier described mechanism. For that we need to evaluate the FEL photon flux. Typical FEL power during each micropulse is $\sim P=8.6$ MW, duration of micropulse is 1 ps and the number of micropulses in one macropulse is around $\sim$5000. When we neglect Er decay during the macropulse (5 μs $\ll\tau_{\mathrm{Er}}\approx1$ ms), then following Eq. (23) and taking into account that under cw diode illumination (power 10 mW) the stationary concentrations of free electrons and holes are $n=p\approx10^{17}$ cm^{-3}, we arrive to the conclusion that $\Delta N_{\mathrm{FEL}}\approx8\times10^{-5}N_{\mathrm{Er}}$. Since the suggested new mechanism does not require formation of a gap state, we assume that all the Er^{3+} ions available in the material can be accessed. The fact that FEL-induced Er PL is characterized by a much longer relaxation time supports the idea that, in this case, another kind of erbium centers are (predominantly) activated than under band-to-band pumping. (We note here that introduction of a donor level, a necessary condition for the "classical" excitation path of Er in Si, enables also efficient nonradiative recombination, e.g., due to the so-called "back-transfer" mechanism.[21]) The PL intensity under pulse excitation should be proportional to the number of excited erbium ions multiplied by a factor $\tau_{\mathrm{eff}}/\tau_{\mathrm{rad}}$, where τ_{eff} and τ_{rad} correspond to the effective and radiative lifetime values of excited Er^{3+} ions, respectively. As mentioned earlier, in view of the much slower decay kinetics one can expect, that in the case of Nd:YAG excitation $\tau_{\mathrm{eff}}/\tau_{\mathrm{rad}}\approx10^{-2}$ and for FEL excitation $\tau_{\mathrm{eff}}/\tau_{\mathrm{rad}}\cong1$. We, therefore, conclude that the proposed excitation mechanism should induce a significantly higher PL intensity than the excitonic one. As can be concluded from Fig. 1, this is indeed observed in the experiment thus providing support for the credibility of the proposed model. We also note that, according to Eq. (23), PL enhancement depends linearly on FEL power, as verified experimentally—see inset to Fig. 1.

The proposed theoretical model in the presented form is valid for the low temperature case. The limitation is imposed by the condition that temperature should be lower than chemical potentials corresponding to the equilibrium carrier concentrations. For the parameters of experiment such limitation gives us $T\lesssim10$ K. The experiment was carried out for $T=4.2$ K that is in the range of validity of our theory. For the investigated case the temperature dependence of the enhancement effect enters only via dependence of the equilibrium carrier concentration on temperature. To describe the observed temperature quenching of the THz-induced PL enhancement effect properly, further development of the model is necessary.

In order to further test the proposed excitation mechanism as the microscopic origin of the observed enhancement of Er PL, dependence of magnitude of the effect on FEL wavelength should be investigated. As given by Eq. (23) and illustrated in Fig. 4, the THz-assisted excitation mechanism has a step-like dependence on FEL wavelength and is characterized by an energy threshold: It is enabled exclusively by photons with energy quantum $\hbar\Omega$ larger than the energy difference between Er excitation and Si bandgap: $\Delta_{ff'}-E_g\approx70$ meV. Experimental observation of this threshold is a major experimental challenge as it lies at the border of FEL range available for the current study. The experiments are currently on the way. The preliminary results for the $\lambda_{\mathrm{FEL}}<16.5$ μm range are shown in the insert to the figure. While definitely more experimental effort is necessary, and the observed behavior differs in detail from the predicted one, a clear variation of the magnitude of the enhancement with FEL wavelength is evident.

VI. CONCLUSION

We propose a plausible microscopic mechanism for explanation of the experimentally observed dramatic increase of the 1.5-μm PL from FZ-Si:Er by THz radiation pulse. We show that this mechanism accounts for all the currently recognized characteristic features of the effect, namely large amplitude, linear dependence on THz photon flux, slow decay kinetics of the induced emission, and thermal quenching. In contrast to the usually considered gap-state mediated excitation mechanism, the proposed energy transfer path opens the way to activate possibly all Er^{3+} ions introduced into the material. Moreover, since it involves participation of the higher-lying second $^4I_{11/2}$ excited state of Er^{3+} ion, a true three-level system is formed, thus opening hopes of realization of population inversion in Si:Er.

Future experiments will test validity of the proposed model and explore further potential of the FEL excitation of Er in FZ-Si for silicon photonics.

ACKNOWLEDGMENTS

We acknowledge the FELIX staff and, in particular, the expert assistance by Dr. Lex van der Meer. The FZ-Si:Er samples were provided by Dr. Frans Widdershoven. The work received financial support of RBRF and the Dutch Scientific Organization NWO. The Amsterdam group was also supported by the European Research Office, US Army. The St. Petersburg group acknowledges support by the grant Russian Scientific Schools.

APPENDIX A: MODEL OF ENERGY-BAND SPECTRUM

Conduction band

The space symmetry group of Si belongs to the class O_h and is nonsymmorphic because it contains elements including nontrivial translations. This property leads to an obligatory double degeneration of the bands at the X point if the spin is neglected.[11] It is known that the two lowest conduction bands of Si are nondegenerate at the Δ point and correspond to the representations Δ_1 and $\Delta_{2'}$, respectively.[10,11] At the X point such representations are compatible with representations X_2 and X_4, using notations of Ref. 11, which have nonzero projection of the momentum matrix element on the axis $\Gamma - X$. Therefore, these doubly degenerated bands have nonzero slope at the X point, which is the reason of the shift of the lowest conduction band minimum from the X point towards the Γ point, but they certainly have zero slope on average.[10,11] More details about the group-theoretical aspects can be found in the book of Bir and Pikus.[11] The minimum of the lowest conduction band $c1$ lies on the (001) axis at distance k_0 from the Γ point and at distance k_X from the X point (see Fig. 2). $k_0 = 0.85(2\pi/a)$ and, therefore, $k_X = 0.15(2\pi/a)$, where $a = 0.543$ nm is the lattice constant of Si. Thus the minumum of $c1$ lies near the X point. According to the group-theoretical considerations[11] [Eq. (30.51)] the Hamiltonian of the conduction band in k-representation can be written as

$$\mathcal{H} = [A_1 k_z^2 + A_2(k_x^2 + k_y^2)]I + A_3 \sigma_x k_x k_y + A_4 \sigma_z k_z, \quad \text{(A1)}$$

where $\vec{k}$ is counted from the X point. σ_x, σ_z are Pauli matrices, and I is identity matrix. Parameters A_1 and A_2 can be found through experimental masses $m_{\|}$, $m_{\perp}$: $A_1 = \hbar^2/2m_{\|}$, $A_2 = \hbar^2/2m_{\perp}$. A_4 is defined through A_1 by position of the minimum of conduction band $c1$ at k_0: $|A_4| = 2A_1 k_X$. Constant A_3 can be expressed through an unknown mass m': $A_3 = \hbar^2/m'$. We have neglected relativistic effects. Therefore the both bands $c1$ und $c2$ are twice degenerate due to the spin. Rewriting Hamiltonian (A1) for $\vec{k}$ counted from the bottom of conduction band $k_z = k_0$ we get

$$H^{c1,c2} = \begin{pmatrix} \varepsilon_1(\vec{k}) & \frac{\hbar^2}{m'} k_x k_y \\ \frac{\hbar^2}{m'} k_x k_y & \varepsilon_2(\vec{k}) \end{pmatrix}. \quad \text{(A2)}$$

Here

$$\varepsilon_1(\vec{k}) = \frac{\hbar^2}{2m_{\|}} k_z^2 + \frac{\hbar^2}{2m_{\perp}}(k_x^2 + k_y^2), \quad \text{(A3)}$$

$$\varepsilon_2(\vec{k}) = \Delta_c + \frac{\hbar^2}{2m_{\|}}(k_z^2 - 4k_X k_z) + \frac{\hbar^2}{2m_{\perp}}(k_x^2 + k_y^2), \quad \text{(A4)}$$

would give energetical spectrum without interaction of the bands. Wave vector $\vec{k}$ is counted from the bottom of conduction band $c1$. The energy gap between conduction bands Δ_c at the minimum of the conduction band $c1$ is given by

$$\Delta_c = 2\frac{\hbar^2}{m_{\|}} k_X^2. \quad \text{(A5)}$$

We get $\Delta_c = 0.5$ eV. To estimate m' we calculate spectrum of (A2)

$$E_{1,2}(\vec{k}) = \frac{1}{2}\Bigg[[\varepsilon_1(\vec{k}) + \varepsilon_2(\vec{k})] \pm \sqrt{[\varepsilon_1(\vec{k}) - \varepsilon_2(\vec{k})]^2 + 4\left(\frac{\hbar^2}{m'} k_x k_y\right)^2} \Bigg]. \quad \text{(A6)}$$

Taking into account that for small k band mixing is small (there is no mixture is z-direction) we have for small k

$$E_1(\vec{k}) = \varepsilon_1(\vec{k}) + \frac{1}{\Delta_c}\left(\frac{\hbar^2}{m'} k_x k_y\right)^2. \quad \text{(A7)}$$

Since the corrugation of conduction band $c1$ is not seen up to carrier concentrations 10^{19} cm^{-3} we get a limitation for parameter m'

$$\left(\frac{m'}{m_{\perp}}\right)^2 \gtrsim \frac{1}{5}\frac{\xi_e}{\Delta_c}, \quad \text{(A8)}$$

from which we have $m' \gtrsim 0.1 m_{\perp}$.

Valence band

For the valence band structure we use a generalization of the Luttinger Hamiltonian in the spherical approximation[17]

$$\mathcal{H} = (A+2B)\hbar^2k^2 - 3B\hbar^2(\vec{k}\cdot\hat{\vec{L}})^2 + \tfrac{1}{3}\Delta\hat{\vec{\sigma}}\cdot\hat{\vec{L}} - \tfrac{1}{3}\Delta. \quad \text{(A9)}$$

Here $\hat{\vec{L}}$ is the unit angular momentum operator, $\hat{\vec{\sigma}}$ is an operator of angular momentum $1/2$, Δ is spin-orbital splitting, and

$$A = -\frac{1}{4}\frac{m_h + m_l}{m_h m_l}, \quad B = -\frac{1}{4}\frac{m_h - m_l}{m_h m_l}, \quad \text{(A10)}$$

where

$$m_h = \frac{m_0}{\gamma_1 - 2\gamma}, \quad m_l = \frac{m_0}{\gamma_1 + 2\gamma}, \quad \text{(A11)}$$

$$\gamma = \tfrac{1}{5}(3\gamma_3 + 2\gamma_2). \quad \text{(A12)}$$

The values of constants γ_1, γ_2, and γ_3 for Si are 4.22, 0.53, 1.38, correspondingly.[22] In the limit of a small spin-orbital splitting $\Delta \to 0$, which can be used for Si, we write Hamiltonian (A9) in the basis of $\Gamma_{25'}$ functions X, Y, Z in k-representation

$$H^{hl} = \hbar^2\begin{pmatrix} (A+2B)k^2 - 3B(k_y^2+k_z^2) & 3Bk_xk_y & 3Bk_xk_z \\ 3Bk_xk_y & (A+2B)k^2 - 3B(k_y^2+k_z^2) & 3Bk_yk_z \\ 3Bk_xk_z & 3Bk_yk_z & (A+2B)k^2 - 3B(k_y^2+k_z^2) \end{pmatrix}. \quad \text{(A13)}$$

The eigenvalues of Hamiltonian (A13) are

$$E_{1,2} = (A-B)\hbar^2k^2 = -\frac{\hbar^2k^2}{2m_h}, \quad \text{(A14)}$$

with corresponding eigenfunctions

$$\psi_1 = \begin{pmatrix} l_x \\ l_y \\ l_z \end{pmatrix}e^{i\vec{k}\vec{r}}, \quad \psi_2 = \begin{pmatrix} m_x \\ m_y \\ m_z \end{pmatrix}e^{i\vec{k}\vec{r}}, \quad \begin{matrix} \vec{l}\perp\vec{k}, \vec{m}\perp\vec{k} \\ \vec{m}\perp\vec{l} \\ l=m=1 \end{matrix} \quad \text{(A15)}$$

for two times degenerated h band, and

$$E_3 = (A+2B)\hbar^2k^2 = -\hbar^2k^2\frac{1}{4}\frac{3m_h - m_l}{m_h m_l}, \quad \text{(A16)}$$

with eigenfunction

$$\psi_3 = \begin{pmatrix} k_x/k \\ k_y/k \\ k_z/k \end{pmatrix}e^{i\vec{k}\vec{r}}, \quad \text{(A17)}$$

for l band. For all three eigenfunctions ψ_1, ψ_2, ψ_3 there are two possible orientations of the spin.

APPENDIX B: OVERLAP INTEGRAL BETWEEN *h* UND *c*2 BANDS

The basis for the Bloch amplitude $u^h_{\vec{k}_2 p_2 s_2}$ are functions $\vec{m}\vec{\Psi}$ and $\vec{l}\vec{\Psi}$, where $\vec{\Psi} = (X, Y, Z)$. Suppose that vector $\vec{k}_2$ has an orientation characterized by angles ϕ and θ in spherical coordinates so that

$$k_{2x} = k_2\cos\theta\cos\phi, \quad k_{2y} = k_2\cos\theta\sin\phi, \quad k_{2z} = k_2\sin\theta. \quad \text{(B1)}$$

Then we can choose for $\vec{m}$, $\vec{l}$

$$m_x = \sin\phi, \quad m_y = -\cos\phi, \quad m_z = 0, \quad \text{(B2)}$$

$$l_x = \sin\theta\cos\phi, \quad l_y = \cos\theta\sin\phi, \quad l_z = -\cos\theta. \quad \text{(B3)}$$

In this case we have

$$\sum_{p_2}|\langle u^h_{\vec{k}_2 p_2 s}|u^{c2,\nu}_{k_0,s_1}\rangle|^2 = \cos^2\theta|\langle Z|xy\rangle|^2\delta_{s_1,s_2}, \quad \text{(B4)}$$

where xy is the wave function of representation $\Delta_{2'}$. The averaging of Eq. (B4) over all possible directions of $\vec{k}_2$ gives

$$\overline{\sum_{p_2}|\langle u^h_{\vec{k}_2 p_2 s_2}|u^{c2,\nu}_{k_0,s_1}\rangle|^2} = \frac{2}{3}|\langle Z|xy\rangle|^2\delta_{s_1,s_2}. \quad \text{(B5)}$$

APPENDIX C: OPTICAL TRANSITION MATRIX ELEMENT

Interaction of electrons with a photon leads to a correction of Hamiltonian (A2). In the lowest order the correction, which induces interband transitions, looks like

$$\hat{H}_{e-r} = \frac{\hbar e}{m'c}\begin{pmatrix} 0 & k_xA_y + k_yA_x \\ k_xA_y + k_yA_x & 0 \end{pmatrix}, \quad \text{(C1)}$$

where $\vec{A} = A_0\vec{e}$, $\vec{e}$ is the vector of polarization and

$$A_0 = \frac{c}{\Omega}\sqrt{\frac{2\pi\hbar\Omega}{\kappa_\infty V}}. \quad \text{(C2)}$$

is the amplitude of the vector-potential of one-photon electromagnetic field. Then we get for the optical transition matrix element

$$\langle \vec{k}' s' | \hat{H}_{e-r} | \vec{k}_1 s_1 \rangle = \sqrt{\frac{2\pi}{\kappa_\infty \hbar \Omega V}} \frac{e\hbar^2}{m'} (k_{1x} e_y + k_{1y} e_x) \delta_{\vec{k}_1, \vec{k}'} \delta_{s_1, s'}. \tag{C3}$$

For unpolarized light we also average over polarization directions

$$\overline{(k_{1x} e_y + k_{1y} e_x)^2} = \tfrac{1}{3}(k_{1x}^2 + k_{1y}^2) = \tfrac{1}{3} k_{1\perp}^2, \tag{C4}$$

where $k_{1\perp}^2 \equiv (k_{1x}^2 + k_{1y}^2)$, and get

$$|\langle \vec{k}' s' | \hat{H}_{e-r} | \vec{k}_1 s_1 \rangle|^2 = \frac{2\pi}{\kappa_\infty \hbar \Omega V} \frac{e^2 \hbar^4}{m'^2} \frac{1}{3} k_{1\perp}^2 \delta_{\vec{k}_1, \vec{k}'} \delta_{s_1, s'}. \tag{C5}$$

[1] A. Polman, J. Appl. Phys. **82**, 1 (1997).

[2] J. Palm, F. Gan, B. Zheng, J. Michel, and L. C. Kimerling, Phys. Rev. B **54**, 17603 (1996).

[3] T. Gregorkiewicz, D. T. X. Thao, J. M. Langer, H. H. P. Th. Bekman, M. S. Bresler, J. Michel, and L. C. Kimerling, Phys. Rev. B **61**, 5369 (2000).

[4] M. Forcales, T. Gregorkiewicz, M. S. Bresler, O. B. Gusev, I. V. Bradley, and J-P. R. Wells, Phys. Rev. B **67**, 085303 (2003).

[5] M. Forcales, T. Gregorkiewicz, I. V. Bradley, and J-P. R. Wells, Phys. Rev. B **65**, 195208 (2002).

[6] T. Gregorkiewicz, D. T. X. Thao, and J. M. Langer, Appl. Phys. Lett. **75**, 4121 (1999).

[7] M. S. Bresler, O. B. Gusev, I. N. Yassievich, and P. E. Pak, Appl. Phys. Lett. **75**, 2617 (1999).

[8] I. Tsimperidis, T. Gregorkiewicz, H. H. P. Th. Bekman, C. J. G. M. Langerak, and C. A. J. Ammerlaan, Mater. Sci. Forum **258–263**, 1497 (1997).

[9] I. Tsimperidis, T. Gregorkiewicz, H. H. P. Th. Bekman, and C. J. G. M. Langerak, Phys. Rev. Lett. **81**, 4748 (1998).

[10] M. Cardona and F. H. Pollak, Phys. Rev. **142**, 530 (1966).

[11] G. E. Pikus and G. L. Bir, *Symmetry and Strain-induced Effects in Semiconductors* (Wiley, New York, 1974).

[12] M. D. Shinn, W. A. Sibley, M. G. Drexhage, and R. N. Brown, Phys. Rev. B **27**, 6635 (1983).

[13] B. K. Ridley, *Quantum Processes in Semiconductors* (Clarendon, Oxford, 1988).

[14] I. N. Yassievich and L. C. Kimerling, Semicond. Sci. Technol. **8**, 718 (1993).

[15] B. R. Judd, Phys. Rev. **127**, 750 (1962).

[16] W. J. Miniscalco, J. Lightwave Technol. **9**, 234 (1991).

[17] V. N. Abakumov, V. I. Perel, and I. N. Yassievich, *Nonradiative Recombination in Semiconductors Modern Problems in Condensed Matter Sciences, Vol. 33*, edited by V. M. Agranovich and A. A. Maradudin (Elsevier, Amsterdam, 1991), pp. 210–213.

[18] F. Priolo, G. Franzó, S. Coffa, and A. Carnera, Phys. Rev. B **57**, 4443 (1998).

[19] M. S. Bresler, O. B. Gusev, B. P. Zakharchenya, and I. N. Yassievich, Phys. Solid State **38**, 813 (1996).

[20] A. Polman, G. N. van der Hoven, J. S. Custer, J. H. Shin, R. Serna, and P. F. A. Alkemade, J. Appl. Phys. **77**, 1256 (1995).

[21] N. Hamelin, P. G. Kik, J. F. Suyer, K. Kikoin, A. Polman, A. Schonecker, and F. W. Saris, J. Appl. Phys. **88**, 5381 (2000).

[22] A. Dargys and J. Kundrotas, *Handbook on Physical Properties of Ge, Si, GaAs and InP* (Science and Encyclopedia Publishers, Vilnius, 1994).